Application of Mass Transfer Theory to Biomarker Capture by Surface Functionalized Magnetic Beads in Microcentrifuge Tubes

Thomas F. Scherr[1], Christine F. Markwalter*[,2], Westley S. Bauer*[,2], David Gasperino[3], David W. Wright[2], Frederick R. Haselton[1,2,#]

[1] Department of Biomedical Engineering, Vanderbilt University, Nashville, TN

[2] Department of Chemistry, Vanderbilt University, Nashville, TN

[3] Intellectual Ventures Laboratory, Bellevue, WA

* These authors contributed equally to this work.

[#] Corresponding author

(E: rick.haselton@vanderbilt.edu; P: 615-322-6622; F: 615-343-7919)

Abstract

In many diagnostic assays, specific biomarker extraction and purification from a patient sample is performed in microcentrifuge tubes using surface-functionalized magnetic beads. Although assay binding times are known to be highly dependent on sample viscosity, sample volume, capture reagent, and fluid mixing, the theoretical mass transport framework that has been developed and validated in engineering has yet to be applied in this context. In this work, we adapt this existing framework for simultaneous mass transfer and surface reaction and apply it to the binding of biomarkers in clinical samples to surface-functionalized magnetic beads. We discuss the fundamental fluid dynamics of vortex mixing within microcentrifuge tubes as well as describe how particles and biomolecules interact with the fluid. The model is solved over a wide range of parameters, and we present scenarios when a simplified analytical expression would be most accurate. Next, we review of some relevant techniques for model parameter estimation. Finally, we apply the mass transfer theory to practical use-case scenarios of immediate use to clinicians and assay developers. Throughout, we highlight where further characterization is necessary to bridge the gap between theory and practical application.

Keywords: mass transfer; surface-functionalized particles; biomarker capture; clinical biomarker assays; numerical modeling

Contents

1. Biomarker Assays in Microcentrifuge Tubes

The microcentrifuge tube is prevalent in microbiology, chemistry, bioengineering, and medicine, and it is arguably the single most commonly used benchtop reaction vessel. In the field of clinical diagnostics, bioseparations are often performed in microcentrifuge tubes using a capture reagent that is specific for an epitope or generic for a class of targets (e.g., proteins, nucleic acids). In biomarker assays, these targets are captured and the amount of target analyte present is quantified. In some cases, the capture reagents are adsorbed to the walls of the tube, but to provide a greater surface area for binding, they are often functionalized onto the surface of a microparticle (Fig. 1). If the microparticle has a magnetic core, bioseparations simply require an applied magnetic field. This has led surface-functionalized magnetic bead-based capture to become an effective component of biochemistry and biomedical assays[5-7], including the isolation of nucleic acids using silica-coated beads[8-14], cell isolation[15], and the extraction of histidine-tagged proteins using immobilized metal affinity ligands[16-20].

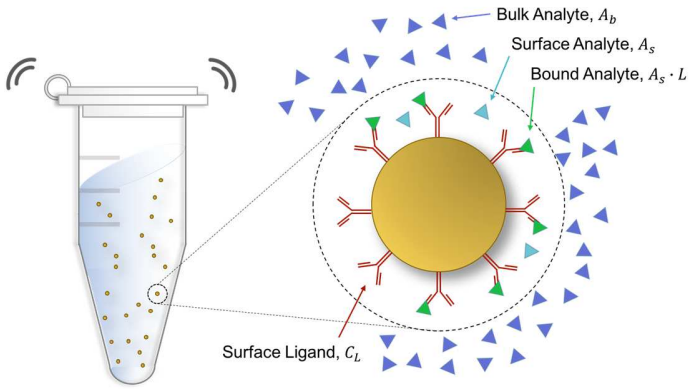

Figure 1. Schematic of analytes binding to functionalized beads in microcentrifuge tubes.

The overall goal of many diagnostic assays is to quantify the presence of a target analyte, and the decisions made during assay development usually attempt to balance accuracy, simplicity, cost, and time. Depending on the processing conditions in a particular assay (such as relative concentrations, binding kinetics, sample fluid properties), a wide variety of outcomes can occur. As a result, biomarker assays that utilize microcentrifuge tubes are typically optimized empirically. This process can be costly, time and labor intensive, and often the parameter space is too large to explore completely.

In this report, we review the underlying transport phenomena present in biomolecular assays that utilize suspended microparticles in microcentrifuge tubes. This

work builds on the extensive development of mass transfer theory in chemical engineering[21-29] and its successful application to the fields of chromatography[30-34] and microfluidics[35-37], where it has been useful for scientists with diverse backgrounds. First we begin with a description of the fluid dynamics of orbital mixing, which includes the common laboratory approach of vortexing. Next, we develop a model for simultaneous mass transfer and surface reaction. Two simplifications to the model result in an analytical solution, and we describe the parameter range in which this algebraic expression is expected to be most accurate. We discuss how the important diagnostic assay parameters can be experimentally estimated. Finally, we present how this approach can be applied in practical use-case scenarios. Throughout, we bring attention to areas for further study and model limitations. We hope that through critical review of the theory, as well as meaningful demonstrations, this broadly applicable framework for biomarker assays will provide a more unifying perspective for the assortment of terminology and fitting models that are currently used throughout the literature.

2. Mixing to Improve Biomarker Capture

Molecular diffusion is a prohibitively slow method for mixing diagnostic assay reagents; therefore, fluid motion is essential. Several laboratory mixing techniques are frequently utilized, including: orbital shaking, magnetic stirring, and rotisserie-style mixing. Each of these approaches result in unique fluid flow characteristics that can affect a biomarker assay[38]. While a similar analysis can be performed for other mixing techniques, this work focuses on one of the most common methods for rapidly mixing samples: vortex mixing.

2.1. Fluid Dynamics in Microcentrifuge Tubes

Vortexing fluids in microcentrifuge tubes is heavily influenced by several key parameters. These classify fluid properties and determine mixing performance. Since it has a large influence on mass transfer, much attention throughout this work will be given to fluid viscosity, η, specifically. The viscosity of many clinically relevant fluids appears to decrease as more shear is applied, and they are labeled “shear-thinning”

fluids[3, 39]. Therefore, when discussing most biofluids, it is more appropriate to speak of an “apparent viscosity”[40], given by eq. (1).

$$\eta_{app} = K\left(\dot{\gamma}_{eff}\right)^{m-1} \quad (1)$$

Here, the apparent viscosity (η_{app}) is a function of the effective strain rate ($\dot{\gamma}_{eff}$) and is defined by a consistency index (K) and a flow behavior index (m), respectively. While the amount of particles in a suspension can affect the apparent viscosity of the suspension[41, 42], in biomarker assays the mass fraction of added surface-functionalized beads is typically low and this effect is usually negligible. Using the apparent viscosity from eq. (1), along with the fluid density (ρ), tube diameter (d_t), and the vortex mixer’s rotational frequency (n), a fluid Reynold’s number (Re_F) can be defined as:

$$Re_F = \frac{\rho n d_t^2}{\eta_{app}}. \quad (2)$$

This dimensionless number is the ratio of inertial forces to viscous forces acting on the fluid. In the context of mass transfer, the fluid Reynolds number assists in the classification of the fluid flow regime (e.g. laminar, transitional, turbulent). As a dimensionless number that takes into account fluid motion, vessel geometry, and fluid properties, the Reynolds number is critically

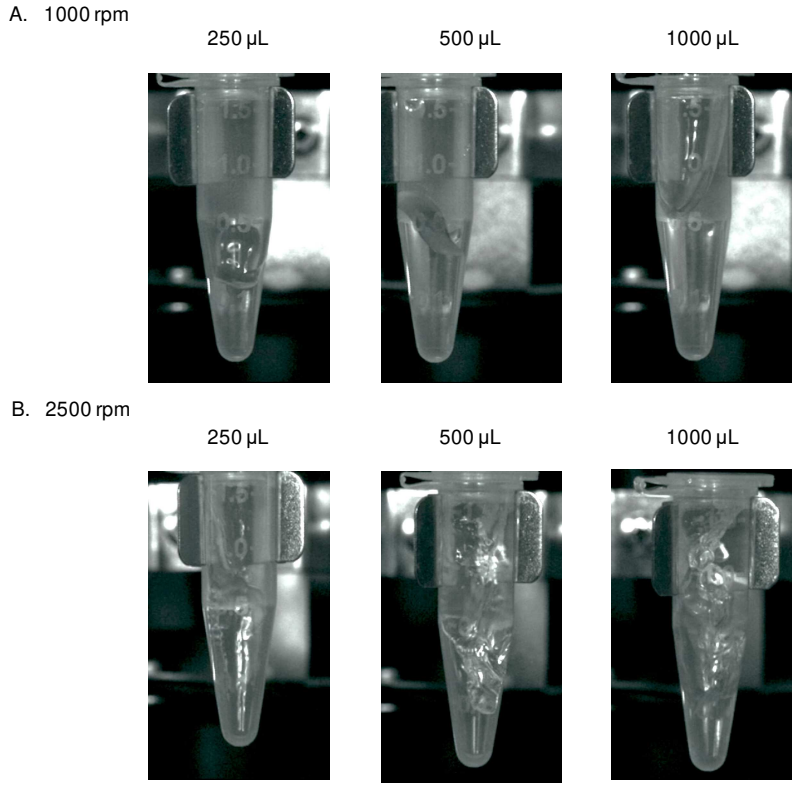

Figure 2. Still images captured from high-speed video of fluid mixing in microcentrifuge tubes at different liquid fill volumes and mixing frequencies: A. 1000 rpm, and B. 2500 rpm.

important in empirical relationships to assist the scale-up of fluid processing vessels. Examples of these correlations include the Power number, which is a measure of power input to the fluid by the agitation method, and the Phase number, a measure of the movement of the bulk liquid compared to the motion of the mixing apparatus[43-45]. The fluid Reynolds number is straightforward to evaluate and can be helpful to classify the general fluid behavior.

In many clinical diagnostic assays, microcentrifuge tubes act as the processing vessel. We can visualize the fluid mixing process during vortex mixing using high speed video (Supplemental Material, still images shown in Fig. 2). Of particular interest are the mixing frequency and the liquid fill volume; high-speed videos show that these two parameters play key roles in fluid motion. At low mixing frequencies, the fluid mixing is "out-of-phase"; the air/liquid interface remains relatively stable during the motion, and the top portion of the fluid "swishes" around the inner walls of the tube while the liquid at the bottom of the tube remains mostly stationary (Fig. 2A). As the frequency increases, "in-phase" motion is observed; fluid mixing is seen throughout the entire depth of the tube (Fig. 2B). Depending on the volume, there is a fundamental difference in the fluid flow pattern. When a microcentrifuge tube that is one-sixth filled is placed on the vortex mixer (250 µL in a 1.5 mL tube), the fluid rapidly climbs the side walls of the conical shaped tube. Throughout the mixing duration, the fluid forms a film that circulates around the walls of the tube. At larger fill volumes (1000 µL of a 1.5 mL tube), the fluid also climbs and circulates along the inner tube walls, but more complex flow patterns are also present. These inertial fluid flow patterns present at higher Reynolds numbers are expected to homogeneously distribute reagents within the fluid, and hence, improve mass transfer to suspended microparticles.

2.2. Particle Behavior During Mixing

Just as fluid motion is necessary to distribute solution phase reagents, a homogenous distribution of beads is necessary to expose these reagents to the full surface area of the beads. When fluid moves around a solid spherical particle during mixing, that particle experiences a number of forces. These particle-fluid interactions can be characterized by three dimensionless numbers: the particle Reynolds number (Re_p), the particle Froude number (Fr), and the Stokes number (St).

$$Re_p = \frac{\rho u_r d_p}{\eta_{app}} \quad (3)$$

$$Fr = \frac{{u_0}^2}{d_p g} \quad (4)$$

$$St = \frac{\rho_p {d_p}^2 u_0}{18 \eta_{app} d_p} \quad (5)$$

The particle Reynolds number, similarly to its fluid companion, is the ratio of inertial forces and viscous forces. Here, the characteristic velocity changes to the relative velocity between the particle and the fluid, u_r, and the characteristic length scale is now the particle diameter, d_p. The particle Froude number indicates the relative scales of inertia to gravity, which is important in understanding particle sedimentation (u_0 is a characteristic velocity, g is the gravitational acceleration constant). The Stokes number relates the time scale of a particle's response to a fluid flow to the characteristic time scale of the fluid flow. Particle Stokes numbers that are very small ($\ll 1$), as is typical of micron-sized beads in biomarker assays, indicate that particles tend to follow fluid streamlines. Still, a certain amount of power must be applied to the fluid to get the particles moving with the fluid and overcome gravitational settling.

There is a long history of literature, mostly resulting from studies on industrial chemistry mixing vessels, that discusses solid particle behavior during mixing processes[46]. Although this literature primarily focuses on large stirred tanks as mixing vessels, much can be gained from inspection of the resulting correlations. The most commonly used criterion for suspension of solid particles in a mixed vessel was proposed by Zwietering[47]:

$$N_S = \frac{S \upsilon^{0.1} {d_p}^{0.2} (g \Delta\rho / \rho_L)^{0.45} x^{0.13}}{D^{0.85}} \quad (6)$$

Here, N_S is the critical impeller speed for "just suspended" particles, S is a function of the mixing impeller in the stirred tank as well as the tank dimensions, υ is the kinematic viscosity of the liquid, d_p is the particle diameter, g is the gravitational acceleration constant, $\Delta\rho$ is the difference between solid and liquid phase densities, ρ_L is the liquid phase density, x is the mass fraction of the solid phase, and D is the mixing tank diameter. This "just suspended" condition defines an impeller speed in a stirred tank at which no particle settles to the bottom of the mixing vessel for more than one second[28]. While this expression is semi-theoretical in nature and must be evaluated

for each mixer, the dependence on fluid and particle properties follows intuition. If the mixing impeller speed was changed to an orbital mixing frequency, analogous correlations could likely be drawn to vortex mixing that would depend on similar parameters: mixing vessel size and geometry, particle size and density, and fluid properties.

While “just suspended” particles are important in industrial chemistry, there has also been a focus on the conditions necessary for complete homogenization of the solid phase – a more desirable condition in bioassay development. The early studies on homogenous particle suspension still focused on large impeller-stirred mixing vessels[48, 49]. Recent studies that used computational fluid dynamics also investigated this problem, but still for large-scale mixing vessels with mechanical agitators[50, 51]. More work must still be done that translates these results to smaller vessels that are mixed by orbital motion, rather than internal impellers. To this end, since the parameters in the fluid Reynolds number are easier to measure when compared to the particle Reynolds number, specifically the fluid mixing frequency instead of the particle-fluid slip velocity, ideally a correlation would be proposed and validated that identifies criteria for homogenization in terms of parameters tangible to assay developers (fluid viscosity, particle diameter, mixing frequency, mixing vessel diameter).

3. Mass Transfer Theory

There are many different modeling approaches that have been taken in the literature to describe mass transport. These models range from simple empirical fits, to theory-driven analytical expressions and full-resolution computational fluid dynamics models. While each of these has an appropriate use, we believe that simpler mathematical models are more likely to be adopted by clinicians and benchtop assay developers. With that in mind, in the following section we develop a lumped (dependent variables are not spatially resolved) theoretical framework that describes simultaneous mass transfer and surface reaction on non-porous functionalized beads. The mass transfer theory that is developed in this report is sufficiently general to be applied to a wide variety of systems, but many of the parameters we apply are specifically relevant to

protein biomarkers of infectious diseases. Numerical solutions were obtained using a 2nd order stiff differential equation solver, in MATLAB (MathWorks, Natick, MA). Appreciating that our intended audience would prefer the simplicity of algebraic expressions over coupled differential equations, we show how simplifications can be made to the model and in what parameter range these simplifications are valid.

3.1. Full Solution

In this system, A_b is an analyte in bulk solution that is transported to the surface of a micron-scale bead. The entire process is illustrated in Figure 1 and summarized by:

$$A_b \leftrightsquigarrow A_S + L \leftrightarrow A_S \cdot L \tag{7}$$

Here, we distinguish unbound analyte on the surface of the bead by the subscript *s*. The analyte undergoes reversible association to an affinity ligand (L), also on the surface of the bead, that results in a ligand-bound analyte, $A_S \cdot L$. For brevity, we will drop the subscript "*s*" and refer to the ligand-bound analyte as $A \cdot L$.

To develop a mathematical framework for these simultaneous processes, we perform a macroscopic balance on each biochemical species:

$$V\frac{dC_{A,b}}{dt} = -k_m a_i\left(C_{A,b} - C_{A,s}\right) \tag{8}$$

$$V\frac{dC_{A,s}}{dt} = k_m a_i\left(C_{A,b} - C_{A,s}\right) - V\left(k_{on}C_{A,s}C_L - k_{off}C_{A\cdot L}\right) \tag{9}$$

$$V\frac{dC_{A\cdot L}}{dt} = V\left(k_{on}C_{A,s}C_L - k_{off}C_{A\cdot L}\right) \tag{10}$$

$$C_L = C_L^0 - C_{A\cdot L} \tag{11}$$

In equations (8-11): V is fluid volume (m^3), $C_{A,b}$ is the concentration of analyte in the bulk solution (mol/m^3), k_m is the mass transfer coefficient between the bulk fluid and the bead surface (m/s), a_i is the surface area of the beads (m^2), k_{on} is the forward reaction rate constant of analyte binding to the ligand (1/M*s), $C_{A,s}$ is the concentration of analyte on the surface (mol/m^3), C_L is the concentration of available ligands for binding (mol/m^3), k_{off} is the reverse rate constant when ligand bound analyte dissociates (1/s), $C_{A\cdot L}$ is the concentration of ligand-bound analyte (mol/m^3), C_L^0 is the initial concentration of ligands (mol/m^3), C_L is the concentration of unbound ligands at time t (mol/m^3). In this lumped model, all biochemical species on the surface of the bead have the same units as the bulk concentration. This resulting system is three first-order, coupled, differential equations, and one algebraic equation that results from a constant number of total

binding sites. While the mass transfer terms are linear, the entire system is non-linear by virtue of the product of concentrations in the reaction terms.

Certain parameters (e.g., rate constants, surface ligand concentration) must be experimentally determined, while others, such as the mass transfer coefficient, can be determined through empirical correlations. Mass transfer to and from particles is a well-studied phenomenon in chemical engineering where fluidized beds have been widely utilized in industrial chemical processes. The Sherwood number, Sh, is defined as the relative ratio of total mass transfer to diffusion over a characteristic length scale, L, and the resulting correlation (one such example from [21] is given as eq. (12)), can provide the corollary equations that complete the model:

$$Sh = \frac{k_m L}{D_{AB}} = 2 + 0.6 Re_p^{\frac{1}{2}} Sc^{\frac{1}{3}} \tag{12}$$

$$Sc = \frac{\eta_{app}}{\rho D_{AB}} \tag{13}$$

The particle Reynolds number, discussed in Section 2, allows mass transfer to account for particle and fluid motion. The Schmidt number, Sc, is the ratio of momentum diffusivity to mass diffusivity, and is defined by the fluid properties.

A considerable number of parameters govern the entire system, namely: sample fluid properties (density, viscosity), ligand surface density, surface area for binding (bead diameter, bead number density), sample volume, kinetic binding rate, kinetic dissociation rate, mixing technique, and initial concentration of bulk analyte. If these parameters are known *a priori*, and in many cases they are known exactly or can be estimated, the model can provide insight into appropriate mixing conditions and incubation times. To simplify analysis, we reduce the model to a two parameter system with the following dimensionless variables:

$$\tilde{C}_{A,b} = \frac{C_{A,b}}{C_{A,b}^0}, \tilde{C}_{A,s} = \frac{C_{A,s}}{C_{A,b}^0}, \tilde{C}_{A\cdot L} = \frac{C_{A\cdot L}}{C_{A,b}^0}, \tilde{C}_L = \frac{C_L}{C_{A,b}^0}, \tau = \frac{t k_m a_i}{V}. \tag{14}$$

Insertion of these dimensionless variables into eqs. (811) results in the following dimensionless parameters:

$$Da^{on} = \frac{V C_{A,b}^0 k_{on}}{a_i k_m}, Da^{off} = \frac{V k_{off}}{a_i k_m} \tag{15}$$

These two Damköhler numbers represent the relative rates of reaction ("on" and "off", respectively) to the rate of mass transfer. Eqs. (8-11) can be re-written in dimensionless form as:

$$\frac{d\tilde{C}_{A,b}}{d\tau} = \tilde{C}_{A,s} - \tilde{C}_{A,b} \quad (16)$$

$$\frac{d\tilde{C}_{A,s}}{d\tau} = \tilde{C}_{A,b} - \tilde{C}_{A,s} + Da^{off}\tilde{C}_{AL} - Da^{on}\tilde{C}_L\tilde{C}_{A,s} \quad (17)$$

$$\frac{d\tilde{C}_{A\cdot L}}{d\tau} = Da^{on}\tilde{C}_L\tilde{C}_{A,s} - Da^{off}\tilde{C}_{AL} \quad (18)$$

$$\tilde{C}_L = \tilde{C}_L^0 - \tilde{C}_{A\cdot L} \quad (19)$$

This most general form of the model makes use of the following assumptions: there are no spatial gradients throughout the system, there is no volume change in the system, and the interfacial area remains unchanged. While these approximations must be loosened in certain industrial chemistry applications, in the context of surface-functionalized beads, these assumptions are valid.

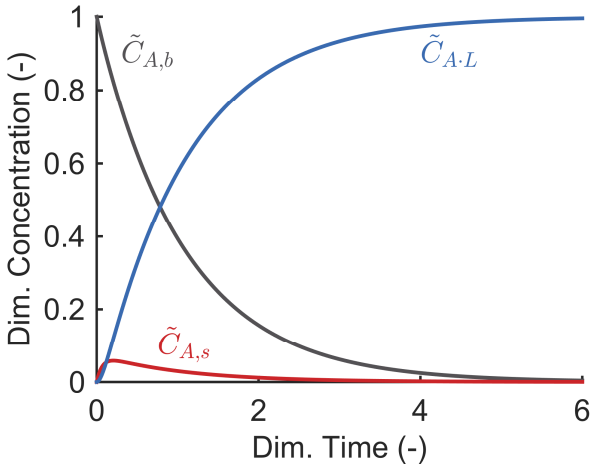

Figure 3. Representative time-series of the three biochemical species in the model. Simulation parameters: Da^{on}=2.633x10^{-4}, Da^{off}=0.0017, $\tilde{C}_L^0$=50000.

The dynamics of a typical system are shown in Fig. 3. Initially, the bulk concentration of analyte ($\tilde{C}_{A,b}$) rapidly decreases and is accompanied by a small, but rapid rise in the concentration of the surface species ($\tilde{C}_{A,s}$) (τ < 0.2). In this time frame, there is minimal binding of target analyte to the capture ligand – only mass transfer from the bulk solution to the surface of the microparticle. As the concentration of surface analyte increases, the bound analyte concentration ($\tilde{C}_{A\cdot L}$) initially lags slightly behind (τ < 0.2). While the concentration gradient between the bulk and surface species tries to replenish the surface analyte available for binding, the binding reaction occurs rapidly on the surface of the bead (0.2 < τ < 2). As a result, the bound target continues its increase, and the surface concentration of analyte is depleted to near zero (2 < τ < 6). The bulk analyte

concentration decreases, which results in a smaller gradient between the bulk and surface concentrations. This results in slower mass transfer and a decrease in the surface concentration. Ultimately, all three biochemical species reach a steady-state value ($\tau > 6$).

3.2. Approximate Analytical Solution

The unbound surface analyte shown in Fig. 3 never goes higher than 10% of the initial bulk analyte concentration, and with the parameters used in Fig. 3, it is negligible after 60 seconds. If the assumption is made that the unbound surface species is at quasi-steady state (QSS), then the system of eqs. (16-19) can be simplified. In addition, it can often be assumed that the ligand is in great excess compared to the analyte, which results in further simplifications to the system:

$$\frac{d\tilde{C}_{A,b}}{d\tau} = \tilde{C}_{A,s} - \tilde{C}_{A,b} \tag{20}$$

$$\frac{d\tilde{C}_{A\cdot L}}{d\tau} = Da^{on}\tilde{C}_L\tilde{C}_{A,s} - Da^{off}\tilde{C}_{AL} \tag{21}$$

$$\tilde{C}_{A,s} = \frac{\tilde{C}_{A,b}+Da^{off}\tilde{C}_{AL}}{Da^{on}\tilde{C}_L+1} \tag{22}$$

$$\tilde{C}_L = \tilde{C}_L^0 \tag{23}$$

In many cases, these two assumptions are justified. The unbound surface concentration may have an initial transient response, but it may quickly reach an equilibrium value where the rates of mass transfer to the surface and the kinetic rates balance each other. Substituting eqs. (22-23) into eqs. (20-21) results in two coupled, but linear ordinary differential equations with the following analytical solution:

$$\tilde{C}_{A,b} = \frac{Da^{on}\tilde{C}_L^0 e^{\frac{-\tau\left(Da^{off}+Da^{on}\tilde{C}_L^0\right)}{Da^{on}\tilde{C}_L^0+1}}}{Da^{off}+Da^{on}\tilde{C}_L^0} + \frac{Da^{off}}{Da^{off}+Da^{on}\tilde{C}_L^0} \tag{24}$$

$$\tilde{C}_{A\cdot L} = -\frac{Da^{on}\tilde{C}_L^0 e^{\frac{-\tau\left(Da^{off}+Da^{on}\tilde{C}_L^0\right)}{Da^{on}\tilde{C}_L^0+1}}}{Da^{off}+Da^{on}\tilde{C}_L^0} + \frac{Da^{on}\tilde{C}_L^0}{Da^{off}+Da^{on}\tilde{C}_L^0} \tag{25}$$

While temporal binding data is important, especially in biomarker assays where time-to-result needs to be minimized, these analytical expressions also give rise to steady-state concentrations at infinite time. Simply by calculating the Damköhler numbers and the dimensionless ligand concentration, the steady-state amount of analyte that can be bound can be calculated from the approximate model as:

$$\tilde{C}_{A\cdot L}^{\infty} = \frac{Da^{on}\tilde{C}_L^0}{Da^{off}+Da^{on}\tilde{C}_L^0}\,. \qquad (26)$$

This concentration allows for prediction of the thermodynamic maximum target analyte that can bind to the surface of the beads. Importantly, this means the unbound bulk species is non-zero and depends on the equilibrium dictated by the “on” and “off” rates.

In Fig. 4, we present a comparison between the full model (eqs. (16-19)) and the approximate analytical solutions (eqs. (24-25)). This enables users to make a quick calculation of the two Damköhler numbers to determine if they are in a region of the phase-space in which the QSS approximation is valid. The color plot in Fig. 4A shows the root-mean squared error between the two solutions. In green regions of the plot, the approximations are valid and the simplified model is sufficient; in the red regions of the

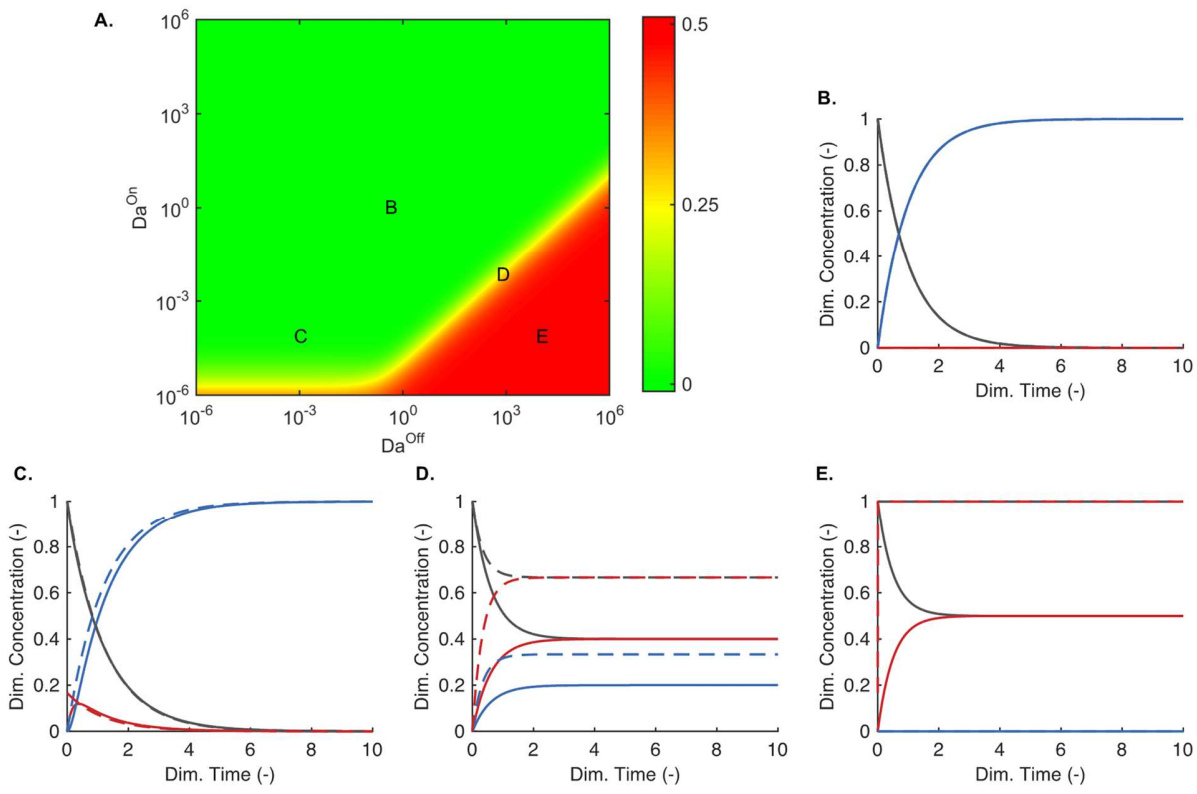

Figure 4. (A) Root mean squared error (red indicates large error, green indicates agreement) between full model and approximation for a range of Da^{on} and Da^{off}, with $\tilde{C}_L$ in large excess ($\tilde{C}_L^0$=50000). (B)-(E) Transient profiles of the three biochemical species in the mass transfer model for Da^{on} and Da^{off}, respectively: (B) 1, 1; (C) 1x10^{-4}, 1x10^{-3}; (D) 1x10^{-2}, 1x10^{3}; (E) 1x10^{-4}, 1x10^{4}. The solid lines represent the full model; the dashed lines represent the approximate solution (Black, bulk analyte; red, unbound surface analyte; blue, ligand-bound surface analyte).

plot, the approximations result in large errors between the simplified model and the full model. Figs. 4B-E show the transient behavior of the individual biochemical species in different regions of the parameter space. When there is an accumulation of unbound analyte on the surface, the approximations used to generate eqs. (24-25) are poor. This typically happens when mass transfer is faster than the forward surface reaction rate, or when the dissociation rate is relatively high. Importantly, this analytical solution holds over a broad range of parameters and can be used for approximations of binding times and steady state concentrations.

3.3. Where More Work is Needed

This lumped model is one approach to understanding mass transfer in biomolecular assays. The literature is rich with empirical correlations of the Sherwood number[23, 24, 26, 27] (see [28] for a thorough review of particle-liquid mass transfer coefficients in stirred tank reactors) that could replace eq. (12). However, these empirical Sherwood number correlations were all determined from large-scale impeller-stirred mixing vessels in industrial chemistry, and it is unclear if any of these will translate to small, vortexed microcentrifuge tubes. Recent efforts to characterize bioreactors in a formal engineering context are an important step towards achieving this clarity[29, 52-56].

The choice of characteristic length and velocity scales is important, and the obvious choices are between the particle and the fluid scale. Since the mass transfer is occurring on the particle scale, the bead diameter and particle-fluid relative velocity would seem appropriate in theory. In practice, however, the use of a particle-fluid relative velocity in the particle Reynolds number makes it a challenging dimensionless group to evaluate. Furthermore, the lumped model presented herein does not resolve mass transfer to an individual particle. Rather, it models mass transfer in the entire domain; this would seemingly make the appropriate length scale the tube diameter. Other variations of the particle Reynolds number that are based on the power input to the mixer or the orbital mixing frequency [28] are easier to calculate and may be appropriate. However, the use of these other variations of the particle Reynolds number in any Sherwood number calculation should be appropriately validated in vortexed microcentrifuge tubes. Once these correlations are well-established and become standard for vortex mixing in microcentrifuge tubes, it will allow easy comparisons

across the literature. The result will be quick dimensionless number calculations that will enter directly into the framework presented.

4. Determination of Model Parameters

A mass transfer model requires accurate parameter estimation for predictive capability. In this section, we briefly describe some of the common methods for determining the necessary parameters (Fig. 5).

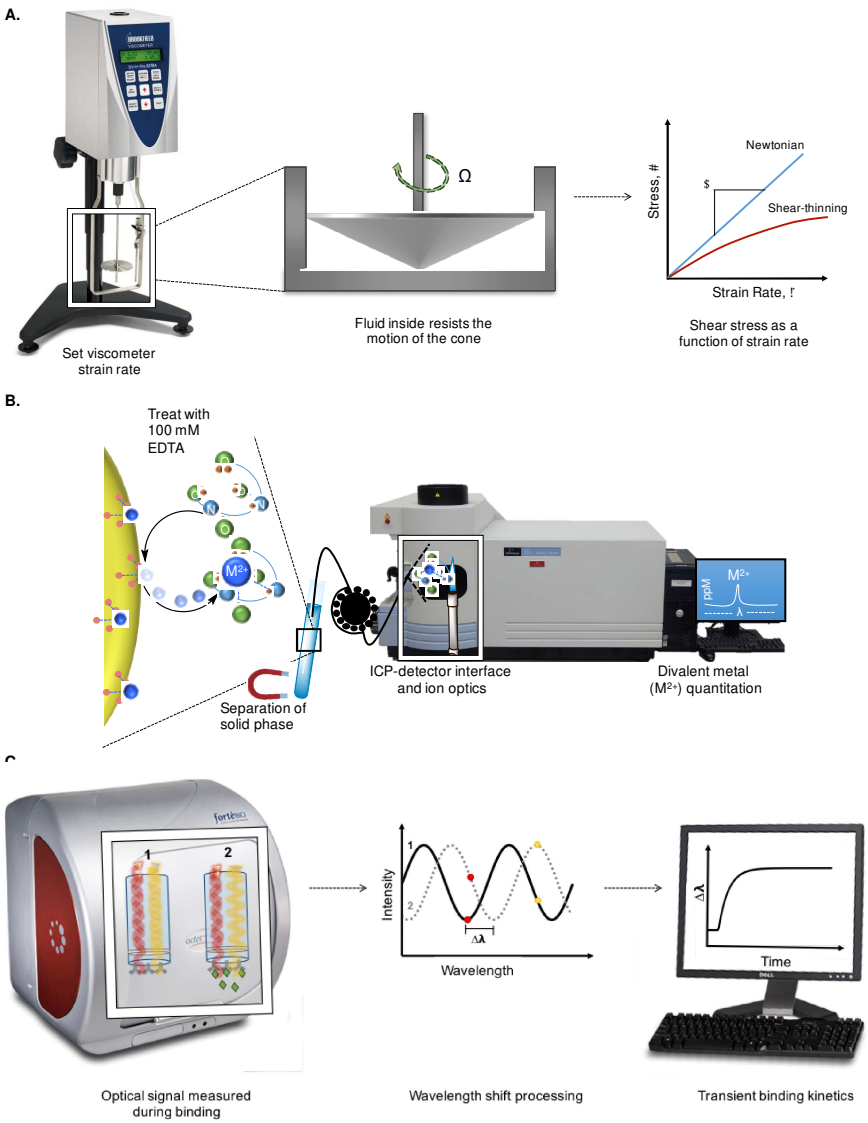

Figure 5. Techniques for mass transfer parameter estimation. (A) A cone and plate viscometer is a common tool to measure the rheological properties of fluids, including shear-thinning bio fluids. (B) Schematic of the process to determine divalent metal concentration using ICP-OES. Immobilized metals are stripped from the solid phase by treatment with EDTA and the chelated metal complex is introduced to the instrument to quantitatively measure metal concentration using a metal specific wavelength. (C) Schematic of biolayer interferometry. White light is sent down a fiber optic sensor. It reflects back to the detector from a stationary reflective layer within the sensor and from the tip of the sensor. When an analyte binds, the distance between the reflective layer and tip of the sensor increases, changing the interference patterns at each wavelength and causing a shift in the resulting interferogram. This phase shift is measured over time and plotted as the binding profile.

4.1. Sample Rheology

Fluid properties, particularly viscosity, are known to influence both mixing and heterogeneous mass transfer in bioprocess engineering[43, 57, 58]. Diffusion is one mode, albeit an inefficient one, of mass transfer. Inspection of the Stokes-Einstein equation (eq. 27), which relates diffusion to fluid viscosity, illustrates how fluid properties affect this mode of mass transfer.

$$D_{AB} = \frac{k_B T}{6\pi\eta_{app} r_a} \quad (27)$$

Here, the diffusion coefficient of molecule *A* within fluid *B* (D_{AB}) is proportional to the Boltzmann constant (k_B) and temperature (T), and inversely proportional to the fluid's apparent viscosity and the hydrodynamic radius of molecule *A* (r_a). In Section 3 we showed that, like diffusion, mass transfer is affected by fluid viscosity. Therefore, for a transport model that requires both a diffusivity and a mass transfer coefficient as inputs, an accurate viscosity is necessary.

Rheological properties can be determined with a viscometer by applying a constant strain rate to the fluid and measuring the shear stress. Cone and plate viscometers (Fig. 5A) are driven at a specific torque for a given strain rate, and sensors measure the resistance to the rotation of a spindle in contact with the fluid. These instruments typically require ~0.5 mL of fluid sample, and have been commonly used to determine rheological properties of biological fluids. If the shear stress response to a change in the strain rate is non-linear, the fluid is categorized as non-Newtonian. As previously noted, many clinically relevant fluids fit the classification of a shear-thinning fluid[3]; the larger the applied strain rate, the lower the apparent viscosity of the fluid. This includes blood, the most-studied biofluid[59-62], and serum, the fluid component of blood after coagulation. Recently, more attention has been devoted to less-invasive biomatrices, such as urine and saliva[8]. These are easy to obtain and typically available in high volumes, which can act to the benefit and detriment of biomarker assays: large volumes are typically easier to handle, but biomarkers are usually at lower concentrations in these matrices. Sputum is another sample matrix used in biomarker assays, particularly for diseases that affect the lungs (e.g. tuberculosis, cystic fibrosis, pneumonia). Collectively, these sample matrices span a wide array of rheological phenomena: urine has properties similar to water and buffer[63]; saliva, while not as viscous as whole

blood, has surfactant-like proteins that make it “frothy” [64]; blood’s non-Newtonian behavior and elastic red blood cells are well known; and sputum is highly-viscous and typically requires pre-treatment to allow for processing. Further rheological characterization of these complex sample matrices will result in more accurate mass transport models.

4.2. Surface Concentration of Ligand

Conjugation of affinity ligands to microbeads generates hybrid materials that are stable in many biological environments and are designed to interact with a specific target. The type of affinity ligand and ligand coverage of a bead governs this bead-target interaction and determines the binding rate of target molecules. Although intuition suggests that labeling beads with the highest possible density of affinity ligands will promote the most effective bead binding to its target, this is often not the case[65-68]. Increasing surface coverage beyond a monolayer is known to induce steric pressure and crowding without adding active binding sites[69, 70], and thus, it is imperative to determine optimum affinity ligand coverage.

Several methods have been employed to quantitatively evaluate ligand coverage. Indirect methods quantify the total number of affinity ligands per bead through supernatant-based assays. In these assays, the number of immobilized affinity ligands per bead can be determined by quantifying the affinity ligand left in the supernatant following a functionalization cycle and comparing this to the initial amount of ligand utilizing mass balance calculations. The number of immobilized affinity ligands per bead can be calculated by dividing the amount of immobilized affinity ligand by the known number of beads. Initial and supernatant affinity ligand concentrations can be determined using biochemical assays such as the bicinchoninic acid assay (BCA assay) and Easy-Titer Antibody Assay Kits. If the affinity ligands absorb in the UV or visible light ranges, such as proteins and nucleic acid sequences, absorbance-based determination can be conducted. According to the Beer-Lambert Law, the amount of light absorbed is proportional to the concentration of the absorbing molecule.

In contrast to supernatant-based assays, direct techniques measure the amount of affinity ligand bound to the surface of the beads. Depending on the size of the capture bead and the affinity ligand being detected, several analytical methods can be used to

quantitatively determine ligand density on the bead. Methods such as gel electrophoresis, which separates complexes based on size and charge, have potential to not only to quantify the amount of affinity ligand on the surface when compared to reference standards, but also to purify[71]. If immobilized metals such as those commonly used in purification of histidine-tagged proteins[16, 20], are used as affinity ligands, inductively coupled plasma optical emission spectrometry (ICP-OES) can be employed to determine metal concentrations. Beads can be treated with a chelating agent, such as ethylenediaminetetraacetic acid (EDTA), to strip all metals from the bead in preparation for analysis (Fig. 5B). Once the metal affinity ligand has been removed from the surface of the bead, a magnet can be used to separate the chelated ligand in solution from the magnetic beads. Figure 5B shows a schematic of this process, followed by metal content analysis with ICP-OES.

While amount of capture ligand on the surface of the beads is an important parameter, the number of active ligands as well as their orientation can affect their apparent kinetics. Therefore, a full characterization of a magnetic bead will include surface ligand quantification, as well as kinetic experiments that will measure the binding performance of a functionalized microparticle.

4.3. Kinetic Parameters

Estimating the kinetic parameters between an analyte and binding ligand is helpful for designing bead-based isolation systems. Selecting binding ligands with the most favorable kinetic parameters can lead to high-affinity interactions that reduce reaction time. There are two types of experiments used to estimate the affinity of biomolecular interactions: (1) equilibrium experiments, and (2) kinetic experiments. In equilibrium experiments, the concentration of one reactant is varied, and the extent of reaction at equilibrium is measured. These steady-state experiments allow one to calculate the equilibrium constant for a reaction (K_{eq}, K_D).

$$A + B \leftrightarrow A \cdot B \tag{28}$$

$$K_{eq} = \frac{1}{K_D} = \frac{k_{on}}{k_{off}} = \frac{C_{A \cdot B}}{C_A C_B} \tag{29}$$

In kinetic experiments, the concentration of one reactant is varied, and the change in reaction rates of the forward and reverse reactions are measured. These transient kinetic experiments are more informative than their equilibrium counterparts, because

analysis of these data yields association and dissociation rate constants (k_{on}, k_{off}) as well as the equilibrium constant[72]. This section will only cover determination of parameters via transient kinetic experiments.

There are several methods by which transient kinetics can be measured. Quartz-crystal microbalance (QCM),[73-76] ellipsometry,[77] surface plasmon resonance (SPR),[78-80] and biolayer interferometry (BLI),[81-83] among others, have all been used to determine kinetic parameters of biomolecular interactions. Commercialization of SPR (BIAcore) and BLI (Fortebio Octet) specifically for application to presteady state kinetic experiments has popularized these techniques for determining kinetic parameters. In SPR, a microfluidic channel delivers analyte to a thin layer of gold functionalized with an affinity ligand. When the analyte binds to the sensor surface, the refractive index at the surface is altered, shifting the phase of the resonant absorbance proportionally[84]. The resulting phase shift is plotted versus time for subsequent data analysis. For BLI (Fig. 5C), white light is sent down a functionalized fiber-optic sensor tip and reflected from a stationary reflective layer within the sensor as well as from the surface of the tip. When analyte binds to the sensor, the distance between the reflective layer and the tip of the sensor increases, shifting the resulting interference pattern[84]. This shift in wavelength can be plotted versus time for subsequent data analysis. In both BLI and SPR, association and dissociation kinetics are observed.

The conditions used in these experiments are idealized and allow for data fitting to simplifications of the mass transfer model that we presented in Section 3. For instance: to determine the forward rate constant for the second-order association reaction in a transient kinetics experiment, sensorgrams are generally fit with pseudo-first order constraints. In this approximation, it is assumed that one reactant (the affinity ligand, *B*) is at much lower concentrations than the analyte, *A*. These simplifications to a complete theoretical model are justified due to the experimental conditions and are desirable when compared to simultaneously fitting a large number of parameters in the full model.

4.4. Where More Work is Needed

These tools provide an experimental framework that is necessary to provide valid parameters for mass transfer models. The common expression with numerical models holds true: “garbage in, garbage out”. While order of magnitude parameters may be

sufficient to approximate assay outcomes with a model, better parameter estimation will result in greater predictive capabilities. As these tools become even more commonplace, a broader catalog of biomolecular kinetic parameters will become available.

Most of these parameters (η_{app}, ρ, D_{AB}, k_{on}, k_{off}) are functions of other variables, including temperature and solution composition. Many biological reagents behave differently in physiological conditions than they do in ambient conditions. For instance, rheological properties of fluids and protein-antibody kinetics are well-known to be highly-dependent on temperature. As a first approximation, and since most diagnostic assays take place in ambient benchtop conditions, these parameters can be measured at room temperature and treated as constants. However, characterization that includes these variables would identify if non-ambient conditions are more optimal. In further regard to kinetic rate constants, to be more beneficial for biomarker assay development, these experiments should include some variation of mixing history (mixing intensity and duration). Correlations of the form

$$k_{on,off} = f(Re_F, MW, \text{structure}) \tag{30}$$

that relate the kinetic binding rate constants to the potential adverse effects of a biomolecule's mixing history along with its properties (size, molecular weight, structure), could be readily implemented in the model presented in this work. These studies would involve a few additional experiments, but would provide a large return on the time and resource investment.

5. Practical Applications and Limitations

Clinicians and bioassay developers will likely be most concerned with practical applications of the theory. In the next section, we show an example from literature that highlights how this theoretical framework was used to design an inexpensive portable mixer for use in bioassays. Next, we solve the complete model under various scenarios pertinent to clinical diagnostics performed in microcentrifuge tubes. This demonstration shows the versatility of this theoretical approach.

5.1. Characterization of an Orbital Mixer for Diagnostics

A similar theoretical analysis to the one presented in Section 3 was recently used to characterize a handheld orbital mixer used in bead-based capture and diagnostic assays (Fig. 6A)[4]. This study used magnetic microbeads with a metal affinity ligand on the surface to capture a histidine-tagged peptide, and the analysis fit mass transfer coefficients at different viscosities to the dimensional equivalent of eq. (24). Qualitatively, the mass transfer coefficient gets smaller at higher viscosities, as expected. The results show that the model fits the experimental kinetic results well over a clinically important range of viscosities. However, there is some disagreement in the steady-state unbound fraction (at long times). This discrepancy could be a result of the model assumptions, particularly the constant capture ligand concentration, or the reduction in kinetic activity in a high shear rate mixer. Nonetheless, this shows how a mass transfer model can be used to characterize a new device used in biomarker assays.

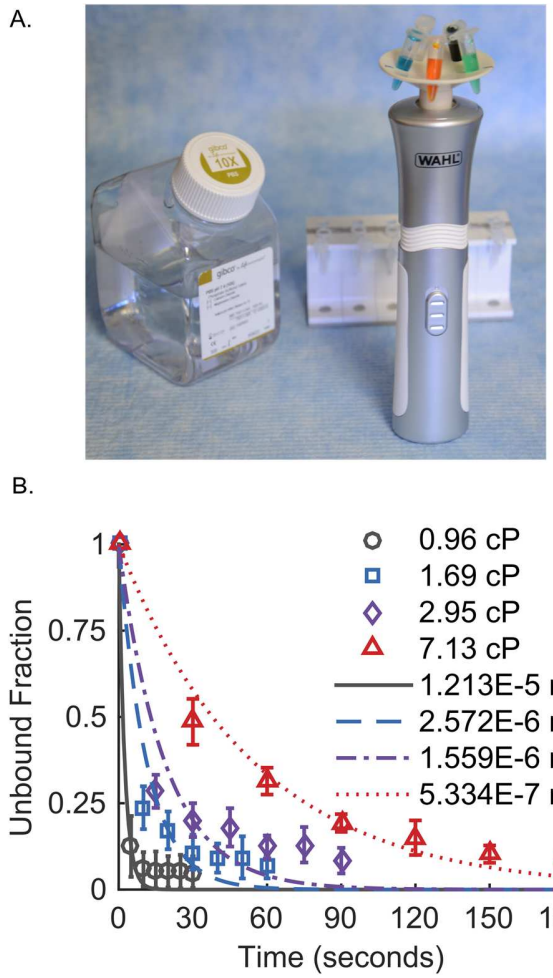

Figure 6. (A) handheld orbital mixer for use in biomarker assays in low-resource settings taken from [4]. (B) The kinetics of biomarker binding in different viscosity fluids. Using fitted mass transfer coefficients in the dimensional equivalents of eq. (24), the mass transfer model shows good agreement with the experimental results.

5.2. Effect of Convective Mixing

The necessity of convective mixing to shorten assay times is widely appreciated in biomarker assays. This is illustrated by the transient responses of bound analyte ($\tilde{C}_{A,b}$) over orders of magnitude changes in Reynolds number, shown in Figure 7. Molecular

diffusion requires no energy input and therefore is the easiest to implement; however, it is a slow process, even in small diameter microcentrifuge tubes. In our model system, less than 20% of the target has been bound from solution after 120 seconds of only diffusion (Re=0). Recall from Section 2 that given a particular fluid and a specific size tube, increasing the frequency of the vortexer (or more generally, mixing speed) increases the Reynolds number. Even a small increase in fluid motion can provide a large improvement in the amount of biomarker that can be captured. To this point, in our model system, a Reynolds number of 1 binds more than 75% of the biomarker after 120 seconds. Increasing the Reynolds number further results in more rapid binding, for instance a Reynolds number of 100 binds >99% of the biomarker in less than 60 seconds. Ultimately, the same steady-state concentration will be reached regardless of the mixing type. However, total assay time is a concern in most clinical diagnostics, and long incubation steps can be avoided by improving the mixing of the beads in the fluid.

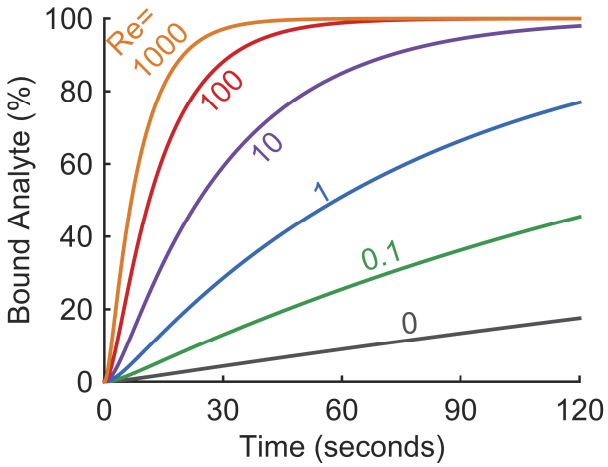

Figure 7. Simulations of the complete mass transfer model showing the importance of convective mixing on bound analyte ($\tilde{C}_{A,b} = 100\% \times \frac{C_{A,b}}{C^0_{A,b}}$). Simulation parameters: Re_p=0-1000, V=250 µL; k_{on}=3.07e4 1/M·s; k_{off}=4.05x10^{-5} 1/s; C^0_L=10.0017x10^{-6} M; $C^0_{A,b}$=200 pM; D_{ab}=7.1795x10^{-11}m/s; V_{slurry}=10 µL; ρ_N=1.025x10^6 beads/µL; d_p=30 µm. Here, V_{slurry} is the volume of the bead slurry added to the sample, ρ_N is the number density of beads in the slurry. Together with d_p, these allow for explicit calculation of total bead surface area, a_i. Using this information, Sh and k_m are calculated by eq. (12). Da^{on} and Da^{off} calculated by eq. (15). The characteristic length scale used for eq. (12) in these simulations was the tube diameter.

5.3. Large Excess of Binding Sites

Surface functionalized beads are typically purchased from a commercial vendor. Unless these beads are modified or fabricated in the lab, the amount of affinity ligand on the surface of the beads is fixed. Therefore, the easiest variable to manipulate in a biomarker assay to obtain more active surface binding sites is the volume of the bead slurry added to the sample. Intuition would suggest that adding more beads to the

sample would result in more rapid capture, and the transient binding results with various bead volumes shown in Figure 8 confirm this. In the model system that we simulated, 100 nL of beads results in less than 35% of bound biomarker ($\tilde{C}_{A,b}$). In this instance, the transfer to the beads is limited due to the lack of total binding sites. As expected, increasing the number of beads, and therefore the number of total surface binding sites, results in more rapid biomarker capture (Fig. 8). While this is desirable, there is a financial consideration as well; larger volumes of functionalized beads come with a higher cost per assay. For instance, comparison of the temporal profiles with 5 µL of beads compared to 10 µL of beads illustrates the diminishing returns of additional binding sites. In this case, doubling the bead volume, will most certainly increase the assay cost; however, doubling the number of available binding sites does not have a substantial impact on the biomarker capture rate. Depending on the surface ligand, which can range from readily available to scarce and valuable, smaller amounts of beads might be necessary to keep total costs low.

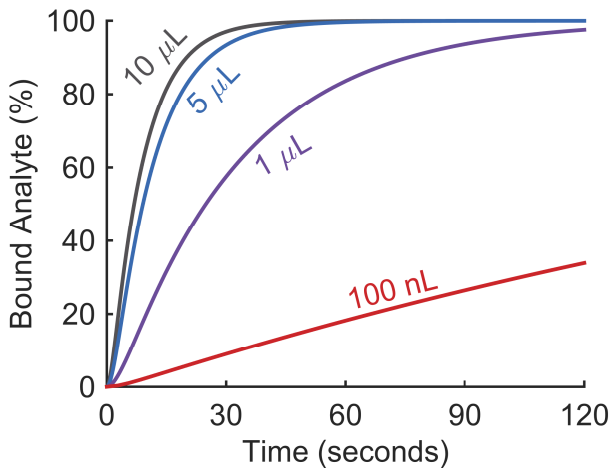

Figure 8. Simulations show increasing the volume of beads added to the sample more rapidly binds target analyte ($\tilde{C}_{A,b} = 100\% \times \frac{C_{A,b}}{C^0_{A,b}}$). Simulation parameters are the same as those used in Figure 7, with the following exceptions: Re is fixed at 1000, and V_{slurry} is varied.

5.4. Effect of Sample Matrix Viscosity

To emphasize the dependence of overall assay time on mixing and sample viscosity, we have solved the full mass transfer model over a range of slip velocities for four clinically relevant biomatrices (Fig. 9). The diffusivity for each fluid was calculated using Stokes-Einstein and is therefore dependent on viscosity. However, viscosities were left as constants in this simulation. Since each of these biofluids are shear-thinning, these are conservative estimates of binding times.

Of principle concern in assays is the time required to bind nearly all of the target biomarkers out of solution, and as such, we have simulated the time required to bind

95% of the target analytes to the surface of beads. Molecular diffusion, with no fluid motion, is substantially slower at all clinically relevant viscosities. As an example, in relatively non-viscous saliva, molecular diffusion (as slip velocity goes to 0) would require nearly 1 hour to bind 95% of the target analyte. Increasing the particle-fluid relative velocity, presumably with faster vortex speeds, beyond 10^{-2} m/s reduces this time to 95% binding to approximately 10 minutes. In blood, increasing the slip velocity from 10^{-4} m/s to 10^{-1} m/s rpm can decrease $t_{95\%}$ from more than 200 minutes to less than 20 minutes, which is a much more reasonable sample preparation time for assays in the field.

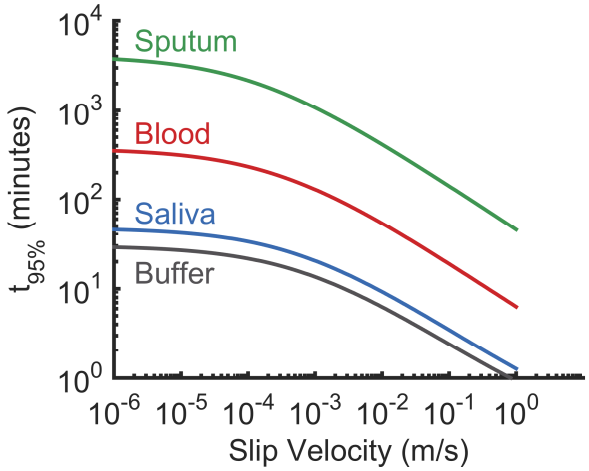

Figure 9. Theoretical time to 95% binding as a function of particle-fluid slip velocity for four clinically relevant biomatrices (buffer, saliva, blood, sputum). The apparent viscosity of each biomatrix was taken from literature[3] and calculated at an apparent shear rate of 10 s^{-1}; all of these biofluids are shear-thinning fluids, and in these simulations the apparent viscosity was not adjusted to account for this. Simulation parameters are the same as those used in Figures 7 and 8, with the following exceptions: V_{slurry} is kept at 10 µL, and Re varies with slip velocity as given by eq. (3). The length scale used in the Sherwood number correlation is the tube diameter.

This demonstrates the potential for mass transfer theory to assist healthcare technicians in selection of appropriate conditions (vortexing frequency, sample dilution to lower viscosity) to meet a target assay time. Additionally, this insight is particularly applicable outside of well-equipped diagnostic laboratories in developed countries. In these resource-limited environments, where high frequency vortexing may not be a viable option, it appears that even a small amount of fluid agitation can result in substantial improvement in biomarker binding. These results also highlight where correlations that relate particle-slip velocity (in the particle Reynolds number) to a more tangible parameter, such as vortex mixer frequency (in the fluid Reynolds number), are appealing and would result in broader model usage.

5.5. Biomolecule Stability During Mixing

The results from the previous sections suggest that the healthcare technician should always set their laboratory vortexer to its maximum setting. Unfortunately, biological reagents can be sensitive to various flow conditions. For instance, there have been reports on the negative correlation between mammalian cell viability and increasing shear[85], as well as reports on shear-induced plasmid DNA degradation[86-88]. Proteins are generally more tolerant of shear, but have been shown to exhibit partial unfolding and eventual aggregation[89-92] or denaturation[93, 94] when partitioned to an air-water interface. This particular problem is a noted challenge in the development of pharmaceuticals and therapeutics[95]. So while increasing the vigor with which a sample is mixed seems ideal, it remains an exercise in empiricism to determine the viability of any biological reagents with the assay.

To illustrate this point, we performed a simple experiment where we measured the effect of harsh mixing on recombinant *Plasmodium* lactate dehydrogenase (rc*p*LDH) (experimental details shown in Appendix). Human LDH levels are measured in liver battery assays[96], but the *Plasmodium* form of LDH is used as a malarial biomarker[97]. It is known to have a complex tertiary and quaternary structure (Fig. 10A), and when recombinantly produced, it is thought to have a deglycosylated form[98]. We anticipated that the combination of these factors would make rc*p*LDH sensitive to harsh mixing. These results reinforce findings by others that above some threshold, biomolecules of interest can be altered by mixing. As the rc*p*LDH was vortexed for longer times, there is a clear decrease in the kinetic "on" rate (Fig. 10B). This decrease in binding kinetics results in

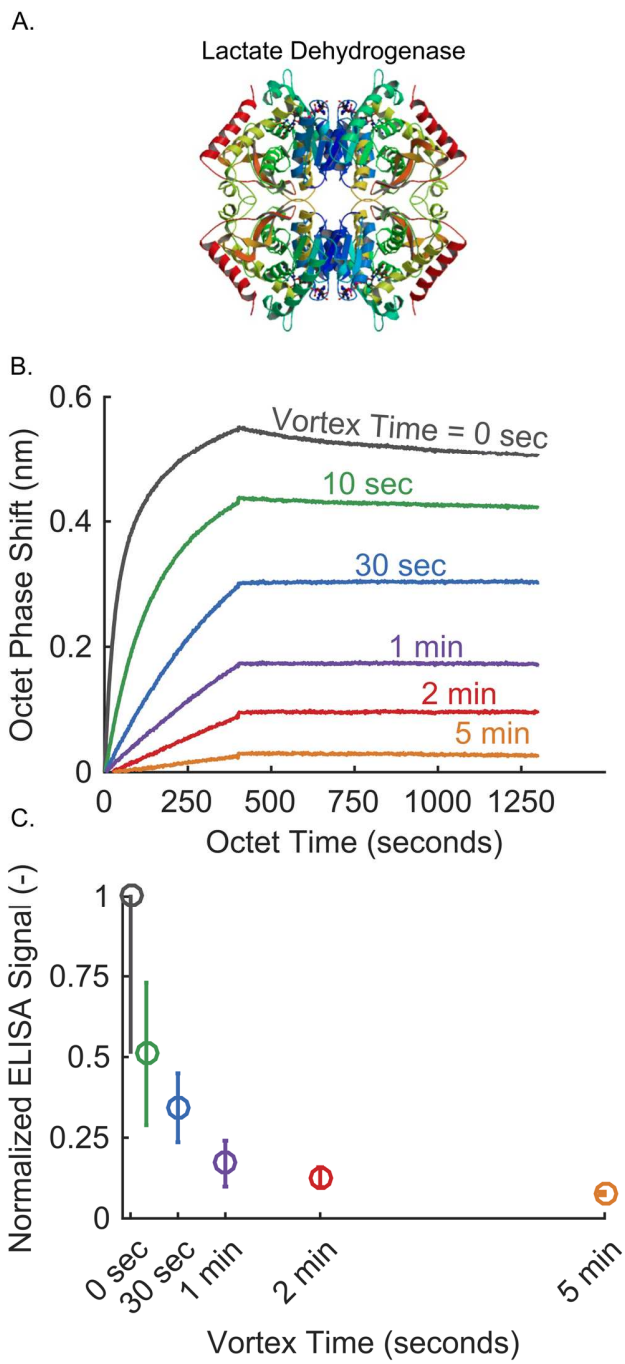

Figure. 10. (A) The biological assembly of pLDH shows a complex tertiary and quaternary structure[1, 2]. (B) As pLDH is vortexed under sub-optimal conditions with a large fluid-air interfacial, the kinetic on-rate of *p*LDH decreases. (C) This kinetic decrease carries through to diagnostic assays that incorrectly give the appearance of lower biomolecule concentrations.

lower signal during a diagnostic enzyme linked immunosorbent assay (ELISA) (Fig. 10C). The operating parameters of this experiment were designed to show a dramatic response: 100 μL of total fluid in a 1.5 mL microcentruge tube and vortexing at a frequency of 3200 rpm. As shown in Fig. 2, small fill volumes mixed at high speeds will result in large air/water interfacial area and that is expected to result in adverse effect on biomolecules. However, this result should inspire caution in the assay developer that wants to leave their benchtop vortexer at its maximum setting.

6. Conclusions

Processing samples with surface-functionalized magnetic beads inside of microcentrifuge tubes is ubiquitous in clinical biomarker diagnostic assays. The capture of a target biomarker is determined by the rates of mass transfer and surface reaction, which are functions of the reagents and the surrounding sample matrix. In this work, we apply a comprehensive theoretical understanding of combined mass transfer and reaction to bead-based analyte capture within a microcentrifuge tube. We have reviewed strategies for estimation of input parameters, relevant model simplifications based on the relative values of these parameters, and the important consequences of the theory. To complete this model and allow easy-to-use expressions for assay developers, further research must be performed to validate correlations for the Sherwood number in small orbitally mixed vessels. In addition, a greater understanding of biomolecule stability in shear flows is needed.

Theoretical modeling efforts and the approximate analytical solutions derived from them, such as the model presented in Section 3 and applied in Section 5, can offer predictive capability and will assist assay developers in choosing operational or fabrication parameters. The system that we have presented should serve as a starting point for future studies on assay development and can be readily modified to include multiple competing reactions or general non-specific interactions that slow the binding or reaction process. As we have demonstrated, this theoretical approach has practical applicability that will be immediately useful to clinicians and assay developers.

7. Acknowledgements

TFS would like to acknowledge support from the Laboratories for Innovation in Global Health Technologies at Vanderbilt University. CFM would like to acknowledge support from the National Science Foundation Graduate Research Fellowship Program under grant 1445197.

8. References

[1] Dunn CR, Banfield MJ, Barker JJ, Higham CW, Moreton KM, Turgut-Balik D, et al. The structure of lactate dehydrogenase from Plasmodium falciparum reveals a new target for anti-malarial design. Nat Struct Biol. 1996;3:912-5.
[2] Dunn CR, Banfield MJ, Barker JJ, Higham CW, Moreton KM, Turgut-Balik D, et al. Plasmodium falciparum L-lactate dehydrogenase complexed with NADH and oxamate. RCSB Protein Data Bank1996. Chapter 09/17/1997.
[3] Scherr TF, Ryskoski HB, Doyle AB, Haselton FR. A two-magnet strategy for improved mixing and capture from biofluids. Biomicrofluidics. 2016;10:024118.
[4] Scherr TF, Ryskoski HB, Sivakumar A, Ricks KM, Adams NM, Wright DW, et al. A handheld orbital mixer for processing viscous samples in low resource settings. Anal Methods-Uk. 2016;8:7347-53.
[5] Gijs MAM. Magnetic bead handling on-chip: new opportunities for analytical applications. Microfluid Nanofluid. 2004;1:22-40.
[6] Gijs MAM, Lacharme F, Lehmann U. Microfluidic Applications of Magnetic Particles for Biological Analysis and Catalysis. Chem Rev. 2010;110:1518-63.
[7] Lim CT, Zhang Y. Bead-based microfluidic immunoassays: the next generation. Biosens Bioelectron. 2007;22:1197-204.
[8] Berry SM, Alarid ET, Beebe DJ. One-step purification of nucleic acid for gene expression analysis via Immiscible Filtration Assisted by Surface Tension (IFAST). Lab on a Chip. 2011;11:1747-53.
[9] Berry SM, Maccoux LJ, Beebe DJ. Streamlining Immunoassays with Immiscible Filtrations Assisted by Surface Tension. Anal Chem. 2012;84:5518-23.
[10] Bordelon H, Adams NM, Klemm AS, Russ PK, Williams JV, Talbot HK, et al. Development of a Low-Resource RNA Extraction Cassette Based on Surface Tension Valves. Acs Appl Mater Inter. 2011;3:2161-8.
[11] Bordelon H, Russ PK, Wright DW, Haselton FR. A Magnetic Bead-Based Method for Concentrating DNA from Human Urine for Downstream Detection. PLoS ONE. 2013;8.
[12] Dineva MA, MahiLum-Tapay L, Lee H. Sample preparation: a challenge in the development of point-of-care nucleic acid-based assays for resource-limited settings. Analyst. 2007;132:1193-9.
[13] LaBarre P, Hawkins KR, Gerlach J, Wilmoth J, Beddoe A, Singleton J, et al. A simple, inexpensive device for nucleic acid amplification without electricity-toward instrument-free molecular diagnostics in low-resource settings. PLoS ONE. 2011;6:e19738.

[14] Strotman L, O'Connell R, Casavant BP, Berry SM, Sperger JM, Lang JM, et al. Selective Nucleic Acid Removal via Exclusion (SNARE): Capturing mRNA and DNA from a Single Sample. Anal Chem. 2013;85:9764-70.
[15] Wang SQ, Tasoglu S, Chen PZ, Chen M, Akbas R, Wach S, et al. Micro-a-fluidics ELISA for Rapid CD4 Cell Count at the Point-of-Care. Sci Rep-Uk. 2014;4.
[16] Knecht S, Ricklin D, Eberle AN, Ernst B. Oligohis-tags: mechanisms of binding to Ni2+-NTA surfaces. J Mol Recognit. 2009;22:270-9.
[17] Bitting AL, Bordelon H, Baglia ML, Davis KM, Creecy AE, Short PA, et al. Automated Device for Asynchronous Extraction of RNA, DNA, or Protein Biomarkers from Surrogate Patient Samples. J Lab Autom. 2015.
[18] Davis KM, Gibson LE, Haselton FR, Wright DW. Simple sample processing enhances malaria rapid diagnostic test performance. Analyst. 2014;139:3026-31.
[19] Davis KM, Swartz JD, Haselton FR, Wright DW. Low-Resource Method for Extracting the Malarial Biomarker Histidine-Rich Protein II To Enhance Diagnostic Test Performance. Anal Chem. 2012;84:6136-42.
[20] Valenti LE, De Pauli CP, Giacomelli CE. The binding of Ni(II) ions to hexahistidine as a model system of the interaction between nickel and His-tagged proteins. J Inorg Biochem. 2006;100:192-200.
[21] Bird RB, Stewart WE, Lightfoot EN. Transport phenomena. Rev. 2nd ed. New York: John Wiley & Sons; 2007.
[22] Russell TWF, Robinson AS, Wagner NJ. Mass and heat transfer : analysis of mass contactors and heat exchangers. Cambridge ; New York: Cambridge University Press; 2008.
[23] Boonlong S, Laguerie C, Couderc JP. Mass-Transfer from Suspended Solids to a Liquid in Agitated Vessels. Chem Eng Sci. 1978;33:813-9.
[24] Armenante PM, Kirwan DJ. Mass-Transfer to Microparticles in Agitated Systems. Chem Eng Sci. 1989;44:2781-96.
[25] Asai S, Konishi Y, Sasaki Y. Mass-Transfer between Fine Particles and Liquids in Agitated Vessels. J Chem Eng Jpn. 1988;21:107-12.
[26] Hughmark GA. Mass Transfer for Suspended Solid Particles in Agitated Liquids. Chem Eng Sci. 1969;24:291-&.
[27] Levins DM, Glastonb.Jr. Application of Kolmogorovs Theory to Particle-Liquid Mass-Transfer in Agitated Vessels. Chem Eng Sci. 1972;27:537-&.
[28] Pangarkar VG, Yawalkar AA, Sharma MM, Beenackers AACM. Particle-liquid mass transfer coefficient in two-/three-phase stirred tank reactors. Ind Eng Chem Res. 2002;41:4141-67.
[29] Scargiali F, Busciglio A, Grisafi F, Brucato A. Mass transfer and hydrodynamic characteristics of unbaffled stirred bio-reactors: Influence of impeller design. Biochem Eng J. 2014;82:41-7.
[30] Gritti F, Guiochon G. A protocol for the measurement of all the parameters of the mass transfer kinetics in columns used in liquid chromatography. J Chromatogr A. 2010;1217:5137-51.
[31] Gritti F, Guiochon G. Mass transfer kinetics, band broadening and column efficiency. J Chromatogr A. 2012;1221:2-40.

[32] Villermaux J. Chemical-Engineering Approach to Dynamic Modeling of Linear Chromatography - a Flexible Method for Representing Complex Phenomena from Simple Concepts. J Chromatogr. 1987;406:11-26.
[33] Traylor SJ, Bowes BD, Ammirati AP, Timmick SM, Lenhoff AM. Fluorescence recovery after photobleaching investigation of protein transport and exchange in chromatographic media. J Chromatogr A. 2014;1340:33-49.
[34] Bowes BD, Koku H, Czymmek KJ, Lenhoff AM. Protein adsorption and transport in dextran-modified ion-exchange media. I: Adsorption. J Chromatogr A. 2009;1216:7774-84.
[35] Gervais T, Jensen KF. Mass transport and surface reactions in microfluidic systems. Chem Eng Sci. 2006;61:1102-21.
[36] Squires TM, Messinger RJ, Manalis SR. Making it stick: convection, reaction and diffusion in surface-based biosensors. Nat Biotechnol. 2008;26:417-26.
[37] Orgovan N, Patko D, Hos C, Kurunczi S, Szabo B, Ramsden JJ, et al. Sample handling in surface sensitive chemical and biological sensing: A practical review of basic fluidics and analyte transport. Adv Colloid Interfac. 2014;211:1-16.
[38] Bai G, Bee JS, Biddlecombe JG, Chen QM, Leach WT. Computational fluid dynamics (CFD) insights into agitation stress methods in biopharmaceutical development. Int J Pharmaceut. 2012;423:264-80.
[39] Truskey GA, Yuan F, Katz DF. Transport phenomena in biological systems. Upper Saddle River, N.J.: Pearson/Prentice Hall; 2004.
[40] Giese H, Klockner W, Pena C, Galindo E, Lotter S, Wetzel K, et al. Effective shear rates in shake flasks. Chem Eng Sci. 2014;118:102-13.
[41] Mueller S, Llewellin EW, Mader HM. The rheology of suspensions of solid particles. P Roy Soc a-Math Phy. 2010;466:1201-28.
[42] Stickel JJ, Powell RL. Fluid mechanics and rheology of dense suspensions. Annual Review of Fluid Mechanics. 2005;37:129-49.
[43] Buchs J, Lotter S, Milbradt C. Out-of-phase operating conditions, a hitherto unknown phenomenon in shaking bioreactors. Biochem Eng J. 2001;7:135-41.
[44] Buchs J, Maier U, Milbradt C, Zoels B. Power consumption in shaking flasks on rotary shaking machines: I. Power consumption measurement in unbaffled flasks at low liquid viscosity. Biotechnology and Bioengineering. 2000;68:589-93.
[45] Buchs J, Maier U, Milbradt C, Zoels B. Power consumption in shaking flasks on rotary shaking machines: II. Nondimensional description of specific power consumption and flow regimes in unbaffled flasks at elevated liquid viscosity. Biotechnology and Bioengineering. 2000;68:594-601.
[46] Rewatkar VB, Joshi JB. Critical Impeller Speed for Solid Suspension in Mechanically Agitated 3-Phase Reactors .2. Mathematical-Model. Ind Eng Chem Res. 1991;30:1784-91.
[47] Zwietering TN. Suspending of solid particles in liquid by agitators. Chem Eng Sci. 1958;8:244-53.
[48] Weisman J, Efferding LE. Suspension of slurries by mechanical mixers. Aiche J. 1960;6:419-26.
[49] Aeschbach S, Bourne JR. The attainment of homogeneous suspension in a continuous stirred tank. The Chemical Engineering Journal. 1972;4:234-42.

[50] Wang S, Jiang M, Ibrahim S, Wu J, Feng X, Duan XX, et al. Optimized Stirred Reactor for Enhanced Particle Dispersion. Chem Eng Technol. 2016;39:680-8.
[51] Calvo S, Delafosse A, Collignon ML, Crine M, Toye D. Experimental Characterisation and Modelling of Homogeneous Solid Suspension in an Industrial Stirred Tank. Adv Mech Eng. 2013.
[52] Garcia-Ochoa F, Gomez E. Bioreactor scale-up and oxygen transfer rate in microbial processes: An overview. Biotechnol Adv. 2009;27:153-76.
[53] Ducci A, Weheliye WH. Orbitally Shaken Bioreactors-Viscosity Effects on Flow Characteristics. Aiche J. 2014;60:3951-68.
[54] Klockner W, Tissot S, Wurm F, Buchs J. Power input correlation to characterize the hydrodynamics of cylindrical orbitally shaken bioreactors. Biochem Eng J. 2012;65:63-9.
[55] Sen A, Kallos MS, Behie LA. Expansion of mammalian neural stem cells in bioreactors: effect of power input and medium viscosity. Dev Brain Res. 2002;134:103-13.
[56] Zhang H, Lamping SR, Pickering SCR, Lye GJ, Shamlou PA. Engineering characterisation of a single well from 24-well and 96-well microtitre plates. Biochem Eng J. 2008;40:138-49.
[57] Giese H, Azizan A, Kummel A, Liao AP, Peter CP, Fonseca JA, et al. Liquid Films on Shake Flask Walls Explain Increasing Maximum Oxygen Transfer Capacities With Elevating Viscosity. Biotechnology and Bioengineering. 2014;111:295-308.
[58] Mcneil B, Harvey LM. Viscous Fermentation Products. Crit Rev Biotechnol. 1993;13:275-304.
[59] Eckmann DM, Bowers S, Stecker M, Cheung AT. Hematocrit, volume expander, temperature, and shear rate effects on blood viscosity. Anesth Analg. 2000;91:539-45.
[60] Lowe GDO, Drummond MM, Lorimer AR, Hutton I, Forbes CD, Prentice CRM, et al. Relation between Extent of Coronary-Artery Disease and Blood-Viscosity. Brit Med J. 1980;280:673-4.
[61] Rand PW, Lacombe E, Hunt HE, Austin WH. Viscosity of Normal Human Blood under Normothermic and Hypothermic Conditions. J Appl Physiol. 1964;19:117-22.
[62] Lowe GDO. Blood Rheology in Arterial-Disease. Clin Sci. 1986;71:137-46.
[63] Inman BA, Etienne W, Rubin R, Owusu RA, Oliveira TR, Rodriques DB, et al. The impact of temperature and urinary constituents on urine viscosity and its relevance to bladder hyperthermia treatment. Int J Hyperthermia. 2013;29:206-10.
[64] Schicht M, Stengl C, Sel S, Heinemann F, Gotz W, Petschelt A, et al. The distribution of human surfactant proteins within the oral cavity and their role during infectious diseases of the gingiva. Ann Anat. 2015;199:92-7.
[65] Elias DR, Poloukhtine A, Popik V, Tsourkas A. Effect of ligand density, receptor density, and nanoparticle size on cell targeting. Nanomedicine. 2013;9:194-201.
[66] Fakhari A, Baoum A, Siahaan TJ, Le KB, Berkland C. Controlling Ligand Surface Density Optimizes Nanoparticle Binding to ICAM-1. J Pharm Sci. 2011;100:1045-56.
[67] Lu Y, Peterson JR, Luais E, Gooding JJ, Lee NA. Surface Epitope Coverage Affects Binding Characteristics of Bisphenol-A Functionalized Nanoparticles in a Competitive Inhibition Assay. J Nanomater. 2015.
[68] Spitznagel TM, Clark DS. Surface-density and orientation effects on immobilized antibodies and antibody fragments. Biotechnology (N Y). 1993;11:825-9.

[69] Saha B, Evers TH, Prins MWJ. How Antibody Surface Coverage on Nanoparticles Determines the Activity and Kinetics of Antigen Capturing for Biosensing. Anal Chem. 2014;86:8158-66.
[70] Zhao X, Pan F, Cowsill B, Lu JR, Garcia-Gancedo L, Flewitt AJ, et al. Interfacial immobilization of monoclonal antibody and detection of human prostate-specific antigen. Langmuir. 2011;27:7654-62.
[71] Aljabali AAA, Barclay JE, Lomonossoff GP, Evans DJ. Virus templated metallic nanoparticles. Nanoscale. 2010;2:2596-600.
[72] Pollard TD. A Guide to Simple and Informative Binding Assays. Mol Biol Cell. 2010;21:4061-7.
[73] Ebara Y, Okahata Y. A Kinetic-Study of Concanavalin-a Binding to Glycolipid Monolayers by Using a Quartz-Crystal Microbalance. Journal of the American Chemical Society. 1994;116:11209-12.
[74] Liu Y, Yu X, Zhao R, Shangguan DH, Bo ZY, Liu GQ. Real time kinetic analysis of the interaction between immunoglobulin G and histidine using quartz crystal microbalance biosensor in solution. Biosensors & Bioelectronics. 2003;18:1419-27.
[75] Okahata Y, Kawase M, Niikura K, Ohtake F, Furusawa H, Ebara Y. Kinetic measurements of DNA hybridisation an an oligonucleotide-immobilized 27-MHz quartz crystal microbalance. Anal Chem. 1998;70:1288-96.
[76] Skladal P, Minunni M, Mascini M, Kolar V, Franek M. Characterization of Monoclonal-Antibodies to 2,4-Dichlorophenoxyacetic Acid Using a Piezoelectric Quartz-Crystal Microbalance in Solution. J Immunol Methods. 1994;176:117-25.
[77] Baleviciute I, Balevicius Z, Makaraviciute A, Ramanaviciene A, Ramanavicius A. Study of antibody/antigen binding kinetics by total internal reflection ellipsometry. Biosensors & Bioelectronics. 2013;39:170-6.
[78] Karlsson R, Falt A. Experimental design for kinetic analysis of protein-protein interactions with surface plasmon resonance biosensors. J Immunol Methods. 1997;200:121-33.
[79] Myszka DG. Kinetic analysis of macromolecular interactions using surface plasmon resonance biosensors. Curr Opin Biotech. 1997;8:50-7.
[80] O'Shannessy DJ, Brigham-Burke M, Soneson KK, Hensley P, Brooks I. Determination of rate and equilibrium binding constants for macromolecular interactions using surface plasmon resonance: use of nonlinear least squares analysis methods. Anal Biochem. 1993;212:457-68.
[81] Smith SA, Silva LA, Fox JM, Flyak AI, Kose N, Sapparapu G, et al. Isolation and Characterization of Broad and Ultrapotent Human Monoclonal Antibodies with Therapeutic Activity against Chikungunya Virus (vol 18, pg 86, 2015). Cell Host Microbe. 2015;18:382-.
[82] Tsibane T, Ekiert DC, Krause JC, Martinez O, Crowe JE, Wilson IA, et al. Influenza Human Monoclonal Antibody 1F1 Interacts with Three Major Antigenic Sites and Residues Mediating Human Receptor Specificity in H1N1 Viruses. Plos Pathog. 2012;8.
[83] Zhang H, de Vries RP, Tzarum N, Zhu XY, Yu WL, McBride R, et al. A Human-Infecting H10N8 Influenza Virus Retains a Strong Preference for Avian-type Receptors. Cell Host Microbe. 2015;17:377-84.
[84] Nirschl M, Reuter F, Voros J. Review of transducer principles for label-free biomolecular interaction analysis. Biosensors (Basel). 2011;1:70-92.

[85] Mcqueen A, Meilhoc E, Bailey JE. Flow Effects on the Viability and Lysis of Suspended Mammalian-Cells. Biotechnol Lett. 1987;9:831-6.
[86] Lengsfeld CS, Anchordoquy TJ. Shear-induced degradation of plasmid DNA. J Pharm Sci. 2002;91:1581-9.
[87] Levy MS, Collins IJ, Yim SS, Ward JM, Titchener-Hooker N, Shamlou PA, et al. Effect of shear on plasmid DNA in solution. Bioprocess Eng. 1999;20:7-13.
[88] Davison PF, Freifeld.D. Lability of Single-Stranded Deoxyribonucleic Acid to Hydrodynamic Shear. J Mol Biol. 1966;16:490-&.
[89] Gidalevitz D, Huang ZQ, Rice SA. Protein folding at the air-water interface studied with x-ray reflectivity. P Natl Acad Sci USA. 1999;96:2608-11.
[90] Frokjaer S, Otzen DE. Protein drug stability: A formulation challenge. Nat Rev Drug Discov. 2005;4:298-306.
[91] Wang W. Protein aggregation and its inhibition in biopharmaceutics. Int J Pharmaceut. 2005;289:1-30.
[92] Wang W, Nema S, Teagarden D. Protein aggregation-Pathways and influencing factors. Int J Pharmaceut. 2010;390:89-99.
[93] Maa YF, Hsu CC. Protein denaturation by combined effect of shear and air-liquid interface. Biotechnology and Bioengineering. 1997;54:503-12.
[94] Wang W. Instability, stabilization, and formulation of liquid protein pharmaceuticals. Int J Pharm. 1999;185:129-88.
[95] Ishikawa T, Kobayashi N, Osawa C, Sawa E, Wakamatsu K. Prevention of Stirring-Induced Microparticle Formation in Monoclonal Antibody Solutions. Biol Pharm Bull. 2010;33:1043-6.
[96] The Merck Manual of Diagnosis and Therapy. 19 ed. Whitehouse Station, NJ: Merck Sharp & Dohme Corp; 2011.
[97] Jain P, Chakma B, Patra S, Goswami P. Potential Biomarkers and Their Applications for Rapid and Reliable Detection of Malaria. Biomed Res Int. 2014.
[98] Palomares LA, Estrada-Mondaca S, Ramirez OT. Production of recombinant proteins: challenges and solutions. Methods Mol Biol. 2004;267:15-52.

9. Appendix: Lactate dehydrogenase stability experimental design

9.1. Materials

Plasmodium falciparum lactate dehydrogenase (*Pf*LDH) was purchased from CTK Biotech (#A3005). Anti-*p*LDH antibodies were purchased from Vista Diagnostics (19g7 and 1201). Horseradish peroxidase was conjugated to 1201 (1201:HRPx) using a conjugation kit (ThermoFisher 31497). For the BLI experiment, 19g7 was biotinylated using EZLink NHS-PEG4-Biotin (ThermoFisher #21329) according to the manufacturer's protocol.

9.2. Methods

Microcentrifuge tubes (1.5 ml, Fisher 05-408-129) containing 100 µl of 1 µM *Pf*LDH in PBS were placed on a Benchmark Vortex Mixer (BV1000) at 3200 rpm for 0, 10 s, 30 s, 1 min, 2 min, 5 min, 10 min, or 30 min.

Binding between the vortexed *Pf*LDH samples and anti-*p*LDH antibody 19g7 was visualized using a Fortebio Octet Red96 system. All solutions were made in 1x phosphate buffered saline (PBS) with 0.02% Tween-20 and 0.1% BSA (Octet buffer) and placed in a black 96-well plate (Griener 655209) 200 µl/well. The BLI experiment consisted of 5 steps: (1) streptavidin biosensors were equilibrated in Octet buffer for 120 s, (2) biotinylated 19g7 (0.5 µg/ml) was loaded onto the tip for 400 seconds, (3) the sensors were placed in Octet buffer for 60 s to achieve a baseline signal, (4) vortexed *Pf*LDH samples (100 nM) were associated to the 19g7-funcitonalized sensors for 400 s, and (5) The sensor tips were placed in Octet buffer for dissociation of *Pf*LDH for 900 s. The experiment was performed at 26C, and the plate was shaken at 1000 rpm to ensure the reaction was not mass transfer-limited.

An ELISA was also performed in order to determine the effect of vortexing on assay signal. Briefly, 100 µl of 2 µg/ml 19g7 in PBS was incubated in an Immulon 2HB 96-well plate for 1 hr. The plate was washed 3x with 1x PBS containing 0.1% Tween-20 (PBST). Next, 300 µl of 15% nonfat dried milk was added to each well, and the plate was incubated for 2 hr. After washing 3x with PBST, 100 µl of vortexed *Pf*LDH samples (500 pM) as well as a *Pf*LDH standard curve (0 – 1.2 nM) in PBST with 0.1% BSA was added to the plate in triplicate and incubated for 2 hours. The plate was washed 5x before 100 µl of 2 µg/ml 1201:HRPx in PBST with 0.5% BSA was added to each well. The plate was covered with foil and incubated for 1 hr before washing 5x with PBST. Finally 100 µl of TMB One solution (Promega G7431) was placed in each well for 10 minutes. The reaction was stopped with 100 µl of 2M H2SO4 and absorbance was measured at 450 nm.

10. Figure Captions

Figure 1. Schematic of analytes binding to functionalized beads in microcentrifuge tubes.

Figure 2. Still images captured from high-speed video of fluid mixing in microcentrifuge tubes at different liquid fill volumes and mixing frequencies: A. 1000 rpm, and B. 2500 rpm.

Figure 3. Representative time-series of the three biochemical species in the model. Simulation parameters: Da^{on}=2.633e-4, Da^{off}=0.0017, $\tilde{C}_L^0$=50000.

Figure 4. (A) Root mean squared error (red indicates large error, green indicates agreement) between full model and approximation for a range of Da^{on} and Da^{off}, with $\tilde{C}_L$ in large excess ($\tilde{C}_L^0$=50000). (B)-(E) Transient profiles of the three biochemical species in the mass transfer model for Da^{on} and Da^{off}, respectively: (B) 1, 1; (C) 1e-4, 1e-3; (D) 1e-2, 1e3; (E) 1e-4, 1e4. The solid lines represent the full model; the dashed lines represent the approximate solution (Black, bulk analyte; red, unbound surface analyte; blue, ligand-bound surface analyte).

Figure 5. Techniques for mass transfer parameter estimation. (A) A cone and plate viscometer is a common tool to measure the rheological properties of fluids, including shear-thinning bio fluids. (B) Schematic of the process to determine divalent metal concentration using ICP-OES. Immobilized metals are stripped from the solid phase by treatment with EDTA and the chelated metal complex is introduced to the instrument to quantitatively measure metal concentration using a metal specific wavelength. (C) Schematic of biolayer interferometry. White light is sent down a fiber optic sensor. It reflects back to the detector from a stationary reflective layer within the sensor and from the tip of the sensor. When an analyte binds, the distance between the reflective layer and tip of the sensor increases, changing the interference patterns at each wavelength and causing a shift in the resulting interferogram. This phase shift is measured over time and plotted as the binding profile.

Figure 6. (A) handheld orbital mixer for use in biomarker assays in low-resource settings taken from [4]. (B) The kinetics of biomarker binding in different viscosity fluids. Using fitted mass transfer coefficients in the dimensional equivalents of eq. (24), the mass transfer model shows good agreement with the experimental results.

Figure 7. Simulations of the complete mass transfer model showing the importance of convective mixing on bound analyte ($\tilde{C}_{A,b} = 100\% \times \frac{C_{A,b}}{C_{A,b}^0}$). Simulation parameters: Re_p=0-1000, V=250 µL; k_{on}=3.07e4 1/M·s; k_{off}=4.05e-5 1/s; C_L^0=10.0017e-6 M; $C_{A,b}^0$=200 pM; D_{ab}=7.1795x10^{-11}m/s; V_{slurry}=10 µL; ρ_N=1.025e6 beads/µL; d_p=30 µm. Here, V_{slurry} is the volume of the bead slurry added to the sample, ρ_N is the number density of beads in the slurry. Together with d_p, these allow for explicit calculation of total bead surface area, a_i. Using this information, Sh and k_m are calculated by eq. (12). Da^{on} and Da^{off} calculated by eq. (15). The characteristic length scale used for eq. (12) in these simulations was the tube diameter.

Figure 8. Simulations show increasing the volume of beads added to the sample more rapidly binds target analyte ($\tilde{C}_{A,b} = 100\% \times \frac{C_{A,b}}{C_{A,b}^0}$). Simulation parameters are the same as those used in Figure 7, with the following exceptions: Re is fixed at 1000, and V_{slurry} is varied.

Figure 9. Theoretical time to 95% binding as a function of particle-fluid slip velocity for four clinically relevant biomatrices (buffer, saliva, blood, sputum). The apparent viscosity of each biomatrix was taken from literature[3] and calculated at an apparent shear rate of 10 s^{-1}; all of these biofluids are shear-thinning fluids, and in these simulations the apparent viscosity was not adjusted to account for this. Simulation parameters are the same as those used in Figures 7 and 8, with the following exceptions: V_{slurry} is kept at 10 µL, and Re varies with slip velocity as given by eq. (3). The length scale used in the Sherwood number correlation is the tube diameter.

Figure. 10. (A) The biological assembly of pLDH shows a complex tertiary and quaternary structure[1, 2]. (B) As pLDH is vortexed under sub-optimal conditions with a large fluid-air interfacial, the kinetic on-rate of *p*LDH decreases. (C) This kinetic decrease carries through to diagnostic assays that incorrectly give the appearance of lower biomolecule concentrations.